Journal of the Korean Society for Nondestructive Testing
Vol. 28, No. 6 (2008. 12)

Analysis of Spin Valve Tunneling Magnetoresistance Sensor for Eddy Current Nondestructive Testing

Dong Young Kim*†, Seok Soo Yoon* and Sang Hun Lee**

Abstract The spin valve tunneling magnetoresistance (SV-TMR) sensor performance is analyzed using Stoner-Wohlfarth model for the detection of eddy current signals in nondestructive testing applications. The SV-TMR response in terms of the applied AC magnetic field dominantly generates the second harmonic amplitude in hard axis direction. The second harmonic eddy current signal detection using SV-TMR sensor shows higher performance than that of the coil sensor at lower frequencies. The SV-TMR sensor with high sensitivity gives a good solution to improve the low frequency performance in comparison with the inductive coil sensors. Therefore, the low frequency eddy current techniques based on SV-TMR sensors are specially useful in the detection of hidden defects, and it can be applied to detect the deeply embedded flaws or discontinuities in the conductive materials.

Keywords: Eddy Current, Magnetoresistance, Nondestructive Testing, Harmonics, Flaw Detection

1. Introduction

The eddy current nondestructive testing uses Faraday's induction law to detect flaws in conductive materials. The primary driving coil carrying an alternating current generating AC magnetic field is placed close to the test specimen to induce an eddy currents in the conductive material. The distortion of eddy currents flow in the conductive material occurs due to the defects or discontinuities, cause a change in the phase and amplitude of the eddy current signal(Cavoit, 2006). This signal can be measured by using a second sensor or inductive probe coil.

The inductive probe coils are the most commonly used sensors for detection of eddy current signal. The sensitivity of inductive coils increases with driving frequency. Therefore, high driving frequency is required for the better eddy current signal performance.

The eddy currents signal mainly depends on the skin depth (δ) or penetration depth such as (Cavoit, 2006)

$$\delta = \frac{1}{\sqrt{\pi \sigma f \mu}} \tag{1}$$

where σ is the conductivity of material, f is the driving frequency, and μ is the magnetic permeability.

Usually, for nondestructive inspection of the conductive materials, the driving frequencies of eddy currents are used in the range of 1 kHz to 3 MHz , and the skin depth is typically between 5 μm and 1 mm or more. Therefore, the eddy current testing with inductive probe coils is useful for detecting near-surface hidden defects because of the skin depth limitations at high

Receved: November 21, 2008, Revised: December 2, 2008, Accepted: December 5, 2008 * Department of Physics, Andong National University, 388 Songchon-dong, Andong, 760-749, Korea ** Department of Radiological Science, Kaya University, 60 Samjeong-dong, Gimhae, 621-748, Korea † Corresponding Author: dykim@andong.ac.kr

frequencies (www.geocities.com).

The magnetic field sensors with high sensitivity at low frequency have been investigated to detect the deeply embedded defects and to overcome limitations in the traditional inductive coil sensors for eddy current nondestructive testing. The magnetoresistance (MR) sensors are promising candidates because their sensitivity is independent of the frequency. These MR sensors can provide higher resolution and deeper penetration for the detection and identification of hidden defects in conductive materials (Dogaru and Smith, 2001; Gilles-Pascaud et al., 2005; Fermon et al., 2006; Wincheski and Namkung, 2000; Dogaru et al., 2001; Dogaru et al., 2000).

In this paper, we analyzed the performance of the eddy current probe based on spin valve tunneling magnetoresistance (SV-TMR) sensor in order to apply at the low frequencies eddy current nondestructive testing.

2. Magnetoresistance

2.1. Magnetoresistance Materials

MR is the property of a magnetic materials that results in a change of resistance with applied magnetic field. The MR materials are being developed for the applications such as hard-disk read heads, magnetic random access memories and magnetic field sensors. The large MR property material can replace the inductive coil sensors in a variety of applications.

The ferromagnetic single layer exhibits an anisotropic magnetoresistance (AMR) (Thomson, 1857). The magnetic thin film multilayer structures can give giant magnetoresistance (GMR) and tunneling magnetoresistance (TMR) effects (Baibich et al., 1988; Binasch et al., 1989; Parkin et al., 2004; Yuasa et al., 2004) and the MR property of these structures are superior than that of the AMR structure. The GMR structure consists of two layers of ferromagnetic metal separated by ultra-thin non-magnetic metal spacer layers. The TMR structures are similar to GMR except that they utilize an ultra-thin insulating layer to separate two magnetic layers rather than a conductor. The GMR and TMR effect occurs is mainly due to the spin-dependent scattering as the current passes from one layer to the other through the spacer layer (Parkin et al., 2004).

The usual figure of merit of MR ratio is traditionally is defined as

$$MR(\%) = \frac{R_{max} - R_{min}}{R_{min}} \times 100 \qquad (2)$$

where R_{max} and R_{min} are the maximum and minimum resistance, respectively. The AMR materials typically have MR ratios about 2-3 %. whereas GMR structures exhibits 20-50 %. While TMR structures commonly can achieve over 200 % of MR ratio using MgO tunnel barrier instead of the usual Al_2O_3 (Parkin et al., 2004; Yuasa et al., 2004).

2.2. Spin Valve TMR Structure

The TMR sensors are usually uses the pinned magnetic layer and a free magnetic layer of the spin valve structures. The spin valve TMR (SV-TMR) structure with MgO insulting layer is shown in Fig. 1(a). The ferromagnetic pinning layer is deposited directly on top of the antiferromagnetic (AFM) layer. The magnetization direction of the pinning layer fixed to the exchange biased direction (H_{ex}). The free layer is

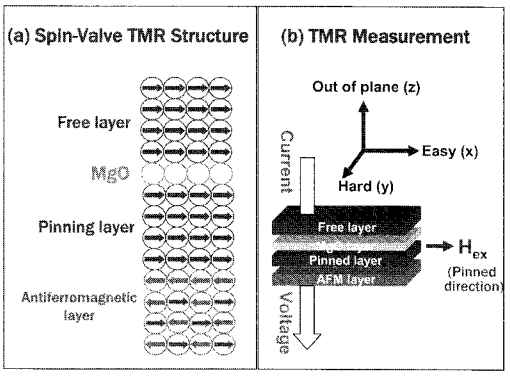

Fig. 1 (a) Spin-valve TMR structure, (b) Schematic diagram of the TMR measurement

separated with pinned layer by MgO layer and it can freely rotate its magnetization direction with respect to the applied magnetic field. The MR changes with applied magnetic field in SV-TMR structure which is measured using the current perpendicular to in-plane configuration with contacts on top and bottom of the film structure as shown in Fig. 1(b).

In SV-TMR structure, the resistance changes with magnetization angle (θ) between pinned and free layers as follows

$$TMR = R_o + \frac{\triangle R}{2}(1 - \cos\theta) \qquad (3)$$

where R_o is the minimum resistance and ΔR is correspond to the difference resistance between maximum and minimum resistance.

The free layer in SV-TMR structure experience the orange peel coupling effect, which is originated from the roughness of the film surface (Kim et al., 2006). This effect shift the hysteresis loop such as the exchange bias effect. The orange peel coupling field (H_{op}) depend on the MgO thickness, which is smaller than the exchange bias field (H_{ex}).

In this paper, we consider the SV-TMR structure for the performance analysis of the eddy current TMR sensor. The magnetic parameters are H_{op} = 10 Oe, anisotropy field H_k = 4 Oe of the free layer, 200 % of TMR ratio and R_o = 1 Ω of minimum resistance, respectively.

The qualitative analyses by using Stoner-Wohlfarth (S-W) model provide a preliminary understanding for the magnetization reversal in the exchange coupled bilayers (Xi et al., 1999). The hysteresis loops of the free layer calculated using the S-W model are shown in Fig. 2 (a) and (c) for the easy and hard magnetic field directions, respectively. In the easy direction, the magnetization with magnetic field shows switching behavior, which is shifted to the positive field direction by the H_{op}. While the magnetization behavior at hard axis shows no hysteresis.

The TMR profiles with applied magnetic field are investigated using eqn. (3) in terms of

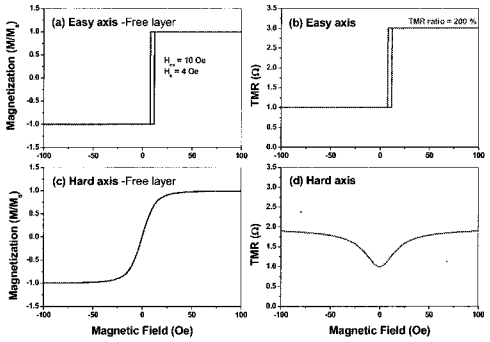

Fig. 2 The hysteresis loop of the free layer in (a) easy and (c) hard axis. The TMR profiles with magnetic field of (b) easy and (d) hard axis in SV-TMR structure

the magnetization angle (θ) of the free layer based on the Stoner-Wohlfarth model calculation. Fig. 3 (b) and (d) show the TMR profiles for the easy and hard magnetic field directions, respectively. In the easy direction, the TMR profile shows switching behavior which is correspond to the hysteresis loop at easy axis in Fig. 3(a). The high TMR at $H > H_{op} + H_k$ is occurred, as the direction of magnetization of the free layer is anti-parallel to that of the pinned layer. The low TMR at $H < H_{op} - H_k$ is occurred, as the two magnetization directions are parallel. The mag- netic field along the easy axis, which is parallel to the pinned layer, decreases the magnetization angle (θ) between two layers and results in decrease the resistance. The magnetic fields in the opposite direction increases the angle, hence increase the resistance.

While the TMR profile at hard axis shows symmetric behavior with no hysteresis as shown in Fig. 3 (d). The magnetic fields along the hard axis, which is perpendicular to the pinned layer, gradually increase the magnetization angle (θ) between two layers up to $\theta = 90^\circ$ and continuously increases the resistance with magnetic field. The maximum resistance change at hard axis which is half value than that of the easy axis.

The hard-disk read heads uses the easy axis TMR properties to detect the two bit magnetic memory information. The TMR response at hard

axis can be applied to the magnetic sensors and it can replace successfully the inductive coil sensors in eddy current nondestructive testing.

3. TMR Signal Analysis

3.1. AC Magnetic Field Effect

In eddy current testing, the sinusoidal AC magnetic field induces the eddy currents in a conducting material being tested such as stainless steel, aluminium etc. The TMR signals under the AC magnetic field are investigated in SV-TMR structure.

Fig. 3 shows the TMR signals with respect to time at hard axis under the applied AC magnetic field H_{ac} = 5 and 40 Oe. The period of the TMR signals at hard axis show only a half cycle that of the driving frequency as shown in Fig. 3 (b) and (c). It means that the TMR signal at hard axis impose second harmonic component dominantly. The TMR signal at H_{ac} = 40 Oe as shown in Fig. 3 (c) is distorted, which indicates that the higher order harmonics are included in the signal. Therefore, we analyzed the higher order harmonic amplitude for the TMR signal at hard axis.

3.2. Harmonics Analysis of TMR Signal

The TMR signals at hard axis are analysed using Fourier transformation to yield the power spectral harmonic amplitudes, $P(nf) = \sqrt{A_n^2 + B_n^2}$, of the signal:

$$S(nf) = A_n \sin(n\omega t) + B_n \cos(n\omega t) \quad (4)$$

where n is the harmonic number, ω is the driving angular frequency ($\omega = 2\pi f$).

Harmonics up to 10th order are calculated by Fourier transformation of TMR signals at H_{ac} = 5 and 40 Oe as shown in Fig. 3. The generation of higher order harmonic amplitude from TMR signals are shown in Fig. 4. The harmonics for driving magnetic field show only first harmonic amplitude, $P(1f)_{TMR}$, which means that the single frequency is used for the AC driving magnetic

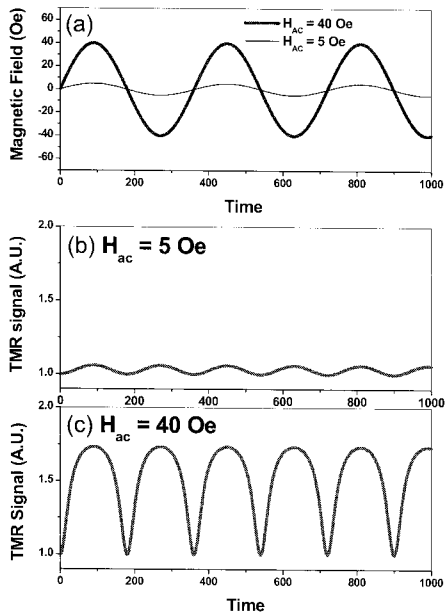

Fig. 3 (a) The driving magnetic field with time and the TMR signals with time at hard axis under the (b) H_{ac} = 5 Oe and (c) H_{ac} = 40 Oe

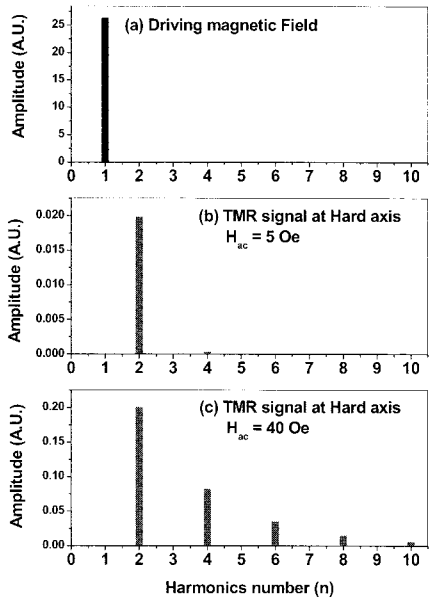

Fig. 4 The higher order harmonic amplitude of (a) driving magnetic field and TMR signal at hard axis under the (b) H_{ac} = 5 Oe and (c) H_{ac} = 40 Oe

field. The harmonics component composed of only even harmonics for the TMR signal at hard axis as sown in Fig. 4 (b) and (c). The even harmonic amplitude drastically decrease with the harmonic number under the H_{ac} = 5 Oe driving magnetic field.

The second harmonic amplitude $P(2f)_{TMR}$ is predominated, and the forth harmonic amplitude $P(4f)_{TMR}$ is negligible. However, the higher order even harmonics under the H_{ac} = 40 Oe driving magnetic field are appeared. These higher even harmonics are generated by the nonlinear behavior of the TMR signal because of the AC driving magnetic field driving above the effective anisotropy field ($H_{eff} > H_{op} + H_k$ = 14 Oe). The dominant second harmonic amplitude of TMR signal at hard axis is useful for the eddy current sensors operation under the AC magnetic field.

3.3. $P(2f)_{TMR}$ with AC Magnetic Field Amplitude

The second harmonic amplitude, $P(2f)_{TMR}$ as a function of AC magnetic field amplitude (H_{ac}) are shown in Fig. 5. The $P(2f)_{TMR}$ at hard axis gradually increases with increasing AC magnetic field up to H_{ac} = 30 Oe beyond that it slightly decreases. The decrease of the $P(2f)_{TMR}$ at high H_{ac} is due to the nonlinear behavior of the TMR signal as shown in Fig. 3 (c). Therefore, If we use the SV-TMR structure with H_{eff} = 14 Oe for the eddy current nondestructive testing, the $P(2f)_{TMR}$ at H_{ac} < 30 Oe is most useful for the SV-TMR sensor applications.

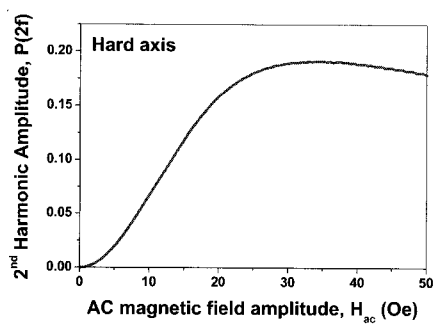

Fig. 5 The second harmonic amplitude, $P(2f)_{TMR}$ with ac magnetic field amplitude, (H_{ac}) at hard axis

4. Eddy Current Signals Based on SV-TMR Sensor

The eddy current testing works by inducing the electrical eddy currents in the conductive materials by applying AC magnetic fields. The defects or flaws within the conductive material distort the flow of the eddy currents. These eddy current signals, V_o can be detected with SV-TMR sensor as shown in Fig. 6.

The eddy current signal is proportional to the H_{ac}, which exponentially decreases with the depth of defects inside the sample due to the penetration depth or the skin depth (δ). Therefore, H_{ac} inside the sample also exponentially decreases with the penetration depth in the conductive material such as.

$$H(d) = H_{ac}\sin(\omega t)e^{-2d/\delta} \tag{5}$$

where d is the depth of the defects from the sample surface. The eddy current signal also reduced by the depth of the defect location.

The penetration depth in eqn.(1) depends on the driving frequency. Therefore, the eddy current signal also depend on the driving frequency. The eddy current signal detected by the inductive coil sensor is proportional to the H_{ac} inside the conductive materials and coil properties as follows

$$V_o(f)_{coil} = 2\pi NAfH_{ac}e^{-2d/\delta} \tag{6}$$

where N is the number of turns of sensor coil, A is the area of the coil. In the case of the

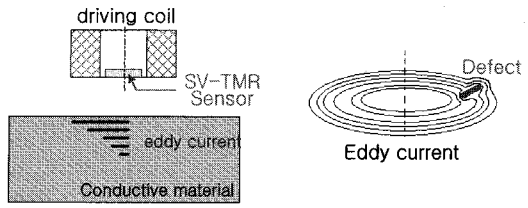

Fig. 6 The schematic diagram of eddy current testing and the distortion of eddy currents at a defect location

inductive coil sensor, the $V_o(f)_{coil}$ proportional to the driving frequency, coil area and number of turns. It means that the high frequency driving and big sensor size is required for the high output signal. The high frequency driving limit the detection of deep defect in thick conductive material being tested by the penetration depth effect.

While, the eddy current signal detected by the SV-TMR sensor is also proportional to the H_{ac} inside the conductive materials and the second harmonic amplitude of SV-TMR response such as

$$V_o(f)_{TMR} = P(2f)_{TMR} H_{ac} e^{-2d/\delta} \qquad (7)$$

where $P(2f)$ is the second harmonic amplitude of SV-TMR response at hard axis. In case of the SV-TMR sensor, the $V_o(f)_{TMR}$ does not depend on driving frequency and sensor size. It means that the low frequency driving and micro-size of sensor is possible for the eddy current sensor applications. The advantage of low frequency driving and micro-size can detect the deep defect and enhance the spatial resolution of the flaws in thick conductive material being tested, respectively.

In order to calculate the eddy current signals of $V_o(f)_{coil}$ and $V_o(f)_{TMR}$, we consider the aluminum material with σ = 1.24 x 10^8 S/m and μ = 1. The calculation parameters are A = 1 cm^2 and N = 100 for the coil sensor and $P(2f)_{TMR}$ = 0.05 x 200 % of TMR ratio for SV-TMR sensor.

Fig. 7 shows the eddy current signal with driving frequency, which are compared with the SV-TMR sensor and inductive coil sensor for the defect depth of d = 0.1, 1 and 10 mm in aluminum material.

For near surface defect (d = 0.1 mm), the eddy current signals by the coil sensor are larger than that of SV-TMR sensor, which is dominant at f > 10 kHz. In the medium depth of d = 1 mm, the eddy current signals by both of coil and SV-TMR sensor are comparable. However, for the deep defect (d = 10 mm), the eddy current signal by SV-TMR sensor is better than that of the coil sensor at the low frequencies. In order to reach the eddy currents up to a depth of 10 mm, a low driving frequency is needed which is less than 100 Hz particularly in case of aluminum materials. The SV-TMR sensor are most advantageous at low-frequencies for detection of deeply buried defects.

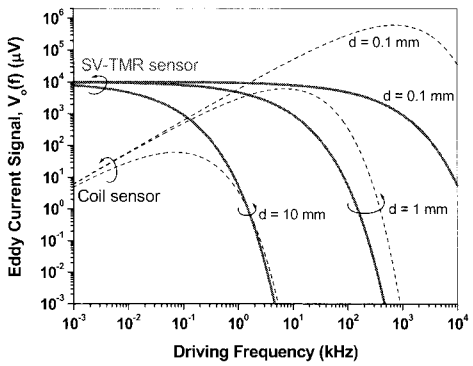

Fig. 7 The eddy current signals with driving frequency are compared with the SV-TMR sensor and coil sensor for the defect depth of d = 0.1, 1 and 10 mm in aluminum material

5. Conclusions

This paper describes the applications of SV-TMR sensor to detect the eddy current signals in nondestructive testing. The TMR signal at hard axis dominantly generate the second harmonic amplitude, which is useful for the eddy current sensors operating under the AC magnetic field at low frequencies.

For near surface defect, the inductive coil sensor is better than that of SV-TMR sensor at the high frequencies. However, for the deeply hidden defects, the SV-TMR sensor is better choice than that of the coil sensor operating at lower frequencies. At lower frequencies, the SV-TMR sensors can easily overcome lower frequency limitations of inductive coil sensors of large size. It is confirmed by our results that high sensitivity eddy current testing can be achieved by using the SV-TMR sensor. Thus,

the low-frequency eddy current techniques based on SV-TMR sensors can be particularly interest used for the detection of hidden defects.

Acknowledgement

This research was supported by a grant from 2008-0085, Academic Research Foundation of Andong National University.

References

Baibich, M. N., Broto, J. M., Fert, A., Nguyen, F. and Petroll, F. (1988) Giant Magnetoresistance of (001)Fe/(001)Cr Magnetic Super-Lattices, *Phys. Rev. Lett.*, Vol. 61 p. 2472

Binasch, G., Grunberg, P., Saurenbach, F. and Zinn, W. (1989) Enhanced Magnetoresistance in Layered Magnetic Structure with Antiferro-magnetic Interlayer Exchange, *Phys. Rev. B*, Vol. 39 p. 2489

Cavoit, C. (2006) Closed Loop Applied to Magnetic Measurements in the Range of 0.1–50 MHz., *Rev. Sci. Instrum.*, Vol. 77, pp. 064703(1-7)

Dogaru, T. and Smith, S. T. (2001) Giant Magnetoresistance Based Eddy Current Sensor, *IEEE Trans. Magn.*, Vol. 37, No. 4, pp. 2790-2793

Dogaru, T., Smith, C. H., Schneider, R. W. and Smith, S. T. (2001) New Directions in Eddy Current Sensing, *Sensors*, Vol. 18, p. 58

Dogaru, T. and Smith, S. T. (2000) Edge Crack Detection Using a Giant Magnetoresistance Based Eddy Current Sensor, *Nondestructive Testing and Evaluation*, Vol. 16, p. 53

Fermon, C., Pannetier, L. M., Biziere, N. and Cousin, B. (2006) Optimized GMR Sensors for Low and High Frequencies Applications, *Sensors and Actuators A: Physical*, Vol. 129, pp. 203-206

Gilles-Pascaud, C., Decitre, J. M., Vacher, F., Fermon, C., Pannetier, M. and Cattiaux, G. (2005) Eddy Current Flexible Probes for Complex Geometries, *QNDE2005 Workshop Proceedings*, Vol. 25A, p 399

Kim, D. Y., Kim, C. G., Kim, C. O., Tsunoda, M. and Takahashi, M. (2006) Effect of Surface Roughness and Field Annealing on Interlayer Coupling in MnIr-based Magnetic Tunnel Junction., *J. Magn. Magn. Mater.*, Vol. 304, pp. e267-e269

Parkin, S. S., Kaiser, C., Panchula, A., Rice, P. M., Hughes, B., Samant, M. and Yang, S. H. (2004) Giant Tunnelling Magnetoresistance at Room Temperature with MgO (100) Tunnel Barries., *Nature Mat.*, Vol. 3 pp. 862-867

Thomson, W. (1857) On the Electrodynamic Qualities of Metals: Effects of Magnetization on the Electric Conductivity of Nickel and Iron, *Proc. Rpy. Soc.* London, Vol. 8, pp. 547-550

www.geocities.com/raobpc/EC-Def.html

Wincheski, B. and Namkung, M. (2000) Deep Flaw Detection with Giant Magnetoresistive (GMR) Based Self-Nulling Probe, QNDE 1999, *AIP Conference Proceedings,* Vol. 509, pp. 465-472

Xi, H., Kryder, M. H. and White, R. M. (1999) Study of the Angular Dependent Exchange Coupling between a F and AF Layers., *Appl. Phys. Lett.,* Vol. 74, p. 2687

Yuasa, S., Nagahama, T., Fukushima, A., Suzuki, Y. and Ando, K. (2004) Giant Room Temperature Magnetoresistance in Single Crystal Fe/MgO/Fe Magnetic Tunnel Barriers., *Nature Mat.,* Vol. 3 pp. 868-871